Type-II Dirac fermions in the PtSe$_2$ class of transition metal dichalcogenides

Huaqing Huang,[1,2] Shuyun Zhou,[1,2] and Wenhui Duan[1,2,3,*]

[1]*Department of Physics, State Key Laboratory of Low-Dimensional Quantum Physics, Tsinghua University, Beijing 100084, China*
[2]*Collaborative Innovation Center of Quantum Matter, Tsinghua University, Beijing 100084, China*
[3]*Institute for Advanced Study, Tsinghua University, Beijing 100084, China*

Recently, a new "type-II" Weyl fermion, which exhibits exotic phenomena, such as an angle-dependent chiral anomaly, was discovered in a new phase of matter where electron and hole pockets contact at isolated Weyl points [Nature (London) **527**, 495 (2015)]. This raises an interesting question about whether its counterpart, i.e., a type-II *Dirac* fermion, exists in real materials. Here, we predict the existence of symmetry-protected type-II Dirac fermions in a class of transition metal dichalcogenide materials. Our first-principles calculations on PtSe$_2$ reveal its bulk type-II Dirac fermions which are characterized by strongly tilted Dirac cones, novel surface states, and exotic doping-driven Lifshitz transition. Our results show that the existence of type-II Dirac fermions in PtSe$_2$-type materials is closely related to its structural $P\bar{3}m1$ symmetry, which provides useful guidance for the experimental realization of type-II Dirac fermions and intriguing physical properties distinct from those of the standard Dirac fermions known before.

Dirac and Weyl fermions, which are basic concepts in high-energy physics, have attracted much attention in condensed-matter physics recently because of the discovery of three-dimensional (3D) Dirac and Weyl semimetals [1–8]. In Dirac and Weyl semimetals, fourfold and twofold degenerate pointlike linear band crossings, the so-called Dirac and Weyl points, appear in the vicinity of the Fermi level. Hence their low-energy excitations are Dirac and Weyl fermions that obey the Dirac or Weyl equations and a large variety of novel phenomena, such as large linear magnetoresistance and a chiral anomaly [9,10], have been predicted and observed in Dirac and Weyl semimetals.

Since the restriction of Lorentz invariance is stringent only in high-energy physics whereas not necessary in condensed-matter physics, Soluyanov *et al.* [11] recently proposed a previously overlooked type of Weyl fermion (type II) that breaks the Lorentz symmetry in condensed-matter systems. Different from conventional Weyl fermions which have standard Weyl points with pointlike Fermi surfaces (which we denote as "type I"), the type-II Weyl fermion emerges at the boundary between electron and hole pockets in materials, such as WTe$_2$ and MoTe$_2$. Such type-II Weyl fermions have recently been theoretically predicted [11,12] and experimentally verified by different research groups [13,14]. The discovery of type-II Weyl fermions not only is of great importance for basic science, but also brings lots of new physical properties, such as an angle-dependent chiral anomaly and topological Lifshitz transitions [11,15,16] that are distinct from the type-I Weyl fermions known before. In the course of searching for new fermions, the following question naturally arose: Is there a Dirac counterpart of the type-II Weyl fermion, namely, a "type-II Dirac fermion," in condensed-matter systems?

So far, several Dirac semimetal materials, such as Na$_3$Bi [1,17] and Cd$_3$As$_2$ [2,18], have been theoretically proposed and experimentally confirmed. However, only conventional type-I Dirac fermions exist in all of these materials.

Here, we predict the existence of type-II Dirac fermions in transition metal dichalcogenides PtSe$_2$, PtTe$_2$, PdTe$_2$, and PtBi$_2$ using first-principles calculations and effective Hamiltonian analysis. Taking PtSe$_2$ as a representative, we find that two symmetry-protected type-II Dirac points are located along the k_z axis in the bulk Brillouin zone (BZ). Different from standard type-I Dirac points with pointlike Fermi surfaces, the type-II Dirac points in PtSe$_2$ appear at the contact of electron and hole pockets with strongly tilted Dirac cones. Furthermore, novel surface states and exotic doping-driven Lifshitz transition occur in these materials. We believe that these materials are promising platforms for the experimental realization of the new type-II Dirac fermions and novel physical properties different from those of standard type-I Dirac semimetals.

All first-principles calculations are carried out within the framework of density-functional theory (DFT) using the Perdew-Burke-Ernzerhof-type [19] generalized gradient approximation for the exchange-correlation functional, which is implemented in the Vienna *ab initio* simulation package [20]. An $8 \times 8 \times 8$ grid of **k** points and a 520-eV plane-wave energy cutoff are adopted for the self-consistent field calculations. Spin-orbit coupling (SOC) is taken into account in our calculations. We construct Wannier functions by projecting the Bloch states from the first-principles calculations of bulk materials onto a set of atomiclike trial orbitals without an iterative maximal-localization procedure [21–24]. Based on the Wannier representation, we further calculate the surface spectral function and Fermi surface of the semi-infinite system using a surface Green's function method [25–27].

As all mentioned materials share similar crystal and electronic structures, we take PtSe$_2$ as a representative material hereafter. PtSe$_2$ crystallizes in a centrosymmetric trigonal crystal structure with space-group $P\bar{3}m1$ (No. 164, D_{3d}^3). The calculated lattice constants are $a = 3.784$ and $c = 5.107$ Å. The atomic structure of PtSe$_2$ is shown in Fig. 1(a). PtSe$_2$ is a periodic stack of layered basic building blocks with weak interlayer interactions. In each layer, Pt atoms are sandwiched by top and bottom Se layers, whereas two Se atoms are related by inversion symmetry. The bulk and surface BZs are shown in
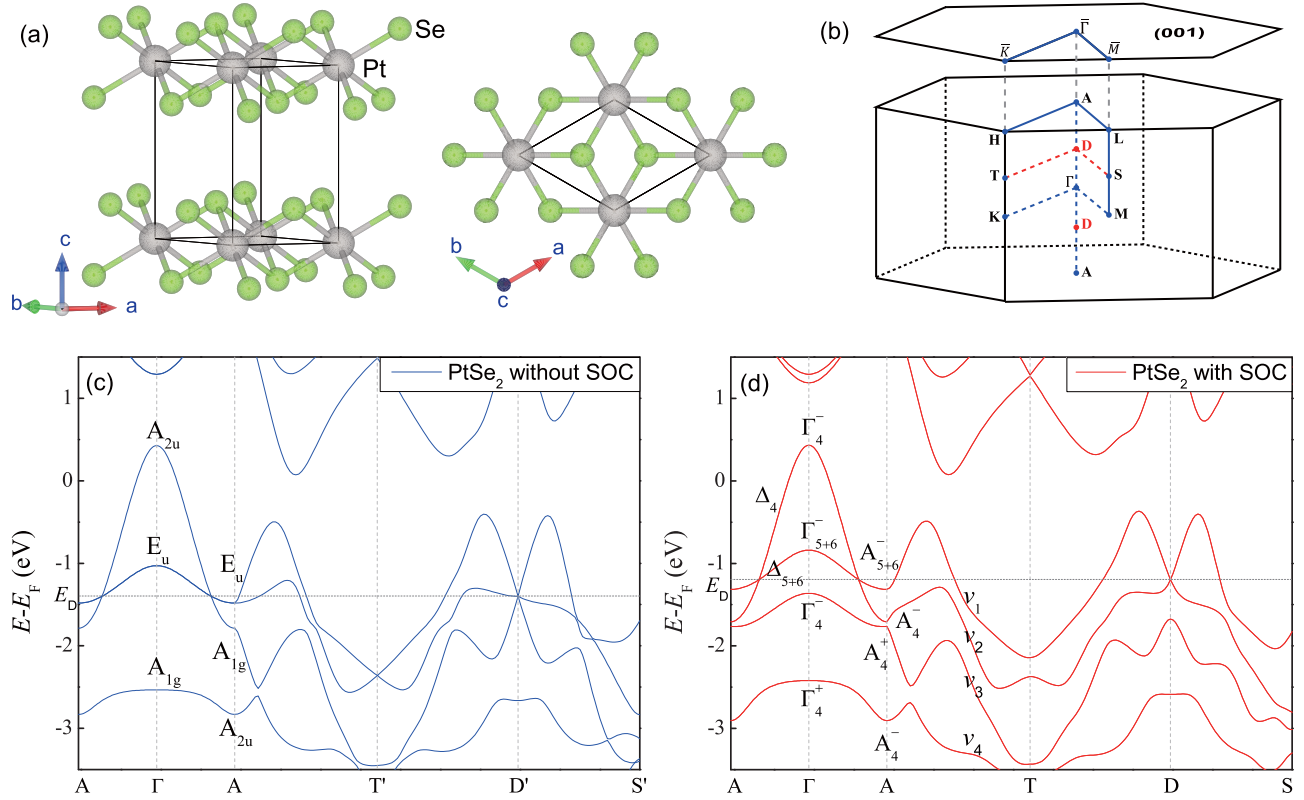
*dwh@phys.tsinghua.edu.cn

FIG. 1. Crystal structure and electronic structure of PtSe$_2$. (a) Crystal structure of PtSe$_2$ with $P\bar{3}m1$ symmetry. (b) BZ of bulk and the projected surface BZs of a (001) surface. The blue dots indicate the high-symmetry points of the BZ, and the red dots highlight the 3D Dirac point position. (c) and (d) The bulk band structures of PtSe$_2$ with/without SOC. The valence bands are labeled as v_i ($i = 1$–4) in terms of their distance to the Fermi level. E_D is the energy of the Dirac points. The irreducible representations of selected bands along the high-symmetric **k** path are indicated.

Fig. 1(b) where high-symmetry points, lines, and Dirac points are also indicated.

We first obtain the band structure of PtSe$_2$ without SOC as shown in Fig. 1(c). There are clear band crossing features near the Fermi level along the Γ-A line. As the two valence bands belong to one-dimensional (1D) irreducible representation (IR) A_2 and two-dimensional (2D) E, respectively, the two bands can simply cross each other without opening a gap. We also check the band crossing along the in-plane S-D-T momentum path [see Fig. 1(b)]. As shown in Fig. 1(c), the doubly degenerate E band split into two bands as the symmetry decreases in this line, hence the band crossing is actually a triply (or sixfold if the spin degree of freedom is considered) degenerate point, which rarely appears in band structures due to the restriction of co-dimension [24] and can be regarded as a new fermion [28,29].

Due to the strong SOC of Pt and Se, including SOC in our first-principles calculations leads to a dramatic modification of the electronic structure as shown in Fig. 1(d). In the presence of SOC, originally degenerate E bands along the Γ-A line split. However, the band crossing still exists with only a small shift of the crossing point. And IRs of the crossing bands become 2D Δ_4, 1D Δ_5, and Δ_6 in the double-point-group $C_{3v}(3m)$ representation of the Γ-A line [30]. Because the Δ_5 and Δ_6 bands are always degenerate due to the coexistence of time reversal and inversion symmetries, the isolated band crossing is a fourfold degenerate Dirac point. More importantly, the

Dirac cone is tilted strongly along Γ-A but untilted along in-plane lines (S-D-T), which is the characteristic feature of the type-II Dirac fermions mentioned above. According to our calculations, a pair of symmetry-related Dirac points is located at the D point, and $\mathbf{k}^c = (0,0,\pm0.319)$ (in units of $2\pi/c$) on the k_z axis with an energy of $E_D = -1.193$ eV below the Fermi level. We also calculate the electronic structures of PtSe$_2$ under uniaxial strain along the c axis, which does not violate the trigonal symmetry of the system, and find that it is possible to tune the Dirac point around the Fermi level by combining external strains with other techniques, such as chemical doping (see the Supplemental Material [31]). Remarkably, the band structures of other PtSe$_2$-class materials (i.e., PtTe$_2$, PdTe$_2$, and PtBi$_2$) are very similar. We have calculated the electronic structures and locations of Dirac points for all materials (see the Supplemental Material [31]). The precise positions of the Dirac points for these materials are summarized in Table I.

Interestingly, there is a band inversion in Γ-A between the third and the fourth valence bands (labeled as v_3 and v_4) with opposite parities, which indicates nontrivial $\mathbb{Z}_2$ topology. We then perform a direct calculation of the $\mathbb{Z}_2$ invariant using the Wannier charge center methods [32] and find $\mathbb{Z}_2 = (1;000)$ for the subspace spanned by valence bands below the v_3 band (i.e., the v_4 band and bands below it) [33].

From the above group-theoretical analysis of the bands, we can clarify that type-II Dirac points exist in the PtSe$_2$ band structure. In order to have a direct visualization of the tilted

TABLE I. The momentum space position $(0,0, \pm k_z^c)$ and energy E_D (with respect to the Fermi level) of Dirac points.

	k_z^c ($2\pi/c$)	E_D (eV)
PtSe$_2$	0.319	−1.193
PtTe$_2$	0.346	−0.860
PdTe$_2$	0.406	−0.545
PtBi$_2$[a]	0.163	2.539
	0.216	2.429

[a]There are two closely located Dirac points in PtBi$_2$: One is of type I, and the other is of type II.

Dirac cone, we plot the 3D band structure on the $k_y = 0$ and $k_z = k_z^c$ planes around the Dirac point. As shown in Figs. 2(a) and 2(b), the two crossing bands exhibit linear dispersions in the vicinity of the Dirac point D along both in-plane and out-of-plane directions. Moreover, the Dirac cone is strongly tilted along the k_z direction, and consequently, a part of the upper cone becomes lower in energy than parts of the lower cone. This unique tilted Dirac cone, which is substantially different from the conventional ones in type-I Dirac semimetals, such as Na$_3$Bi and Cd$_3$As$_2$ [1,2], is similar to that of the recently discovered type-II Weyl fermion in WTe$_2$ and MoTe$_2$ [11–14]. Therefore, the pair of Dirac points in PtSe$_2$ can be regarded as 3D type-II Dirac points. The existence of type-II Dirac

points in PtSe$_2$ suggests that new kinds of quasiparticle type-II 3D Dirac fermions which are different from the standard 3D Dirac fermions discovered before, can emerge in this material. Many physical properties of PtSe$_2$, such as magnetotransport anomalies, would be significantly different from those of type-I Dirac semimetals.

Next we study the Fermi-surface topology and possible Lifshitz transition in PtSe$_2$ as the chemical potential varies. Dirac semimetals were previously thought to have a pointlike Fermi surface at the Dirac point, and the Fermi surface expands to closed spheres or ellipsoids after n or p doping, which were observed in Na$_3$Bi and Cd$_3$As$_2$ by recent experiments [17,18]. However, the Fermi surface of PtSe$_2$ shows quite different features when the chemical potential is fine-tuned around the Dirac point. The bottom projections of Figs. 2(a) and 2(b) show the isoenergy contour of electron and hole pockets when the chemical potential is shifted to E_D. It is clear that the Dirac point appears as the contact point between electron and hole pockets on the k_x-k_z plane [Fig. 2(a)] while the pockets shrink to the single Dirac point at the $k_z = k_z^c$ plane [Fig. 2(b)]. This can be also seen in the evolution of the 3D isoenergy surface as the chemical potential passes through E_D. As shown in Fig. 2(c), when $E_F < E_D$, there is a hole pocket with threefold rotation symmetry at the center of the bulk BZ. The electron pockets are divided into two parts: The inner one consists of two half cones which disconnect
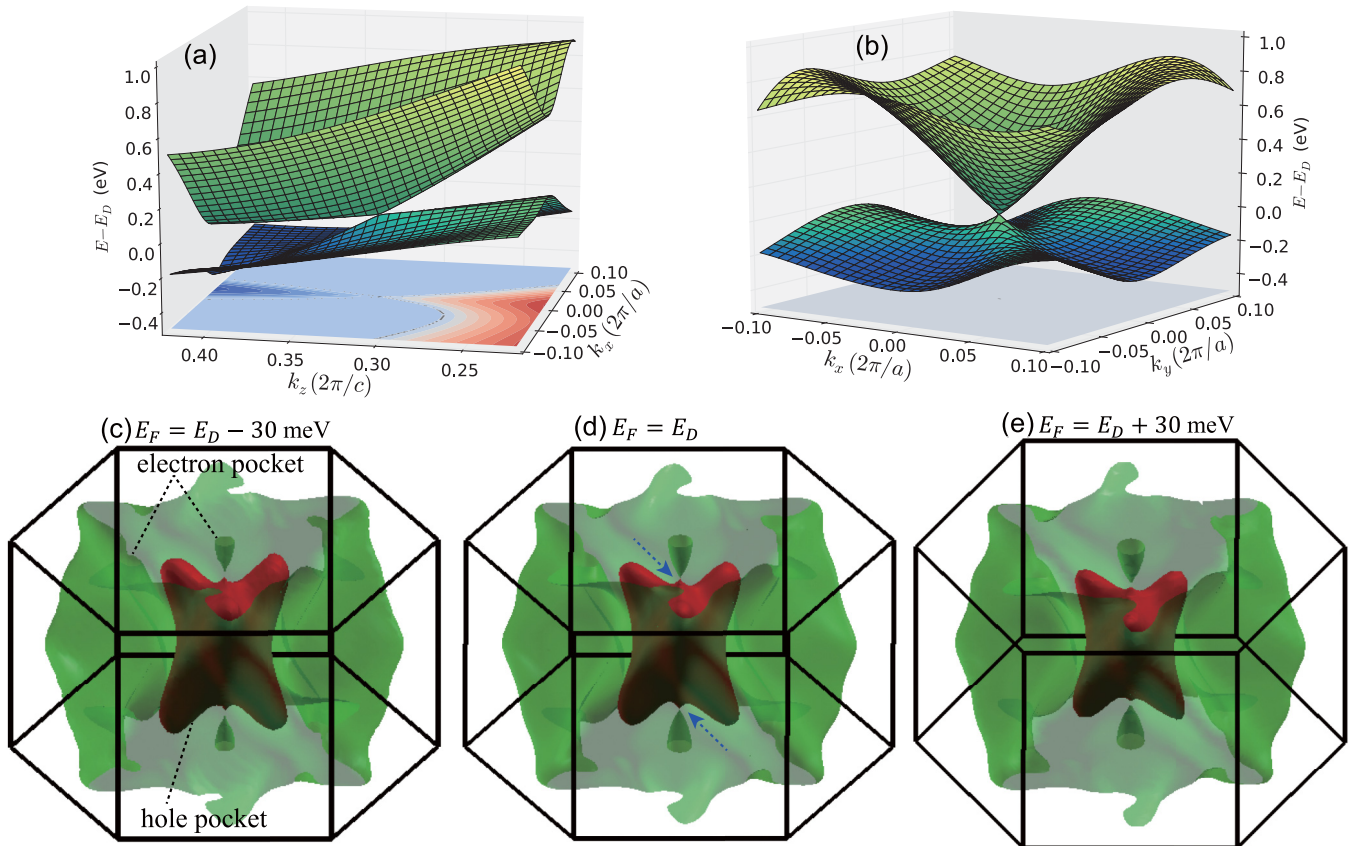

FIG. 2. Type-II Dirac points in PtSe$_2$. (a) and (b) Three-dimensional band structures on the (a) k_x-k_z plane and (b) $k_z = k_z^c$ plane around the Dirac point. The bottom projection shows the isoenergy contour of electron and hole pockets with respect to E_D. (c)–(e) Three-dimensional isoenergy surface at (c) $E_F = E_D - 30$ meV, (d) E_D, and (e) $E_D + 30$ meV. Contact between electron and hole pockets occurs at the Dirac points (marked with blue arrows) when $E_F = E_D$.

with the hole pocket; whereas the outer one has the lantern shape surrounding other pockets. When the chemical potential increases to the energy of the Dirac point $E_F = E_D$, the hole pocket touches two inner electron pockets at the Dirac points as illustrated in Fig. 2(d). Further increasing the chemical potential disconnects the electron and hole pockets again, and the hole pocket vanishes gradually [see Fig. 2(e)]. Evidently, the isoenergy surface evolves rapidly and undergoes a change in topology (i.e., Lifshitz transition) with tuning the chemical potential around the Dirac point. Therefore the Dirac point that emerges at the boundary between electron and hole pockets and possible Lifshitz transition on the Fermi surface can be readily observed when the chemical potential is brought down to the Dirac point by doping or other techniques [31].

To further reveal the nature of type-II Dirac points in PtSe$_2$, we derive the low-energy effective Hamiltonian using the theory of invariants [34]. The first-principles calculations indicate that the wave functions of low-energy valence-band states at the Γ point are mostly from the Se-$4p_{x,y,z}$ orbitals. Due to the C_3 rotation and inversion symmetries of the system, it is more convenient to make a linear combination of these orbitals as $|\eta, p_{x\pm iy}, s\rangle$ and $|\eta, p_z, s\rangle$, where $\eta = \pm$ for bonding and antibonding states and $s = \uparrow\downarrow$ for spin. By including spin-orbit coupling in the above atomic orbital picture, we need to consider the total angular momentum, and thus the new eigenstates at the Γ point can be written as $|J = \frac{3}{2}, J_z = \pm\frac{3}{2}\rangle$, $|J = \frac{3}{2}, J_z = \pm\frac{1}{2}\rangle$, and $|J = \frac{1}{2}, J_z = \pm\frac{1}{2}\rangle$.

At the Γ point, the top two valence-band states belong to 2D IR Γ_4^- and degenerate 1D IRs $\Gamma_5^- + \Gamma_6^-$, respectively (see Fig. 1). The basis functions of these IRs are mainly composed of $|\frac{1}{2}, \pm\frac{1}{2}\rangle$ and $|\frac{3}{2}, \pm\frac{3}{2}\rangle$ according to their double-group representations [30]. In terms of the above four basis states (on the order of $|\frac{3}{2}, \frac{3}{2}\rangle$, $|\frac{1}{2}, -\frac{1}{2}\rangle$, $|\frac{3}{2}, -\frac{3}{2}\rangle$, and $|\frac{1}{2}, \frac{1}{2}\rangle$), we can construct an effective 4×4 Hamiltonian by considering the time-reversal, inversion, and D_{3d}^3 symmetries [1],

$$H_{\rm eff}(\mathbf{k}) = \epsilon_0(\mathbf{k}) + \begin{pmatrix} M(\mathbf{k}) & Ak_+ & 0 & B(\mathbf{k}) \\ Ak_- & -M(\mathbf{k}) & -B(\mathbf{k}) & 0 \\ 0 & -B^*(\mathbf{k}) & M(\mathbf{k}) & Ak_- \\ B^*(\mathbf{k}) & 0 & Ak_+ & -M(\mathbf{k}) \end{pmatrix},$$

where $\epsilon_0(\mathbf{k}) = C_0 + C_1 k_z^2 + C_2(k_x^2 + k_y^2)$, $M(\mathbf{k}) = M_0 - M_1 k_z^2 - M_2(k_x^2 + k_y^2)$, $B(\mathbf{k}) = B_3 k_z k_+^2$, and $k_\pm = k_x \pm ik_y$. The material-dependent parameters in the above Hamiltonian are determined by fitting the energy spectrum of the effective Hamiltonian with that of DFT calculations. Our fitting yields $C_0 = -0.2079$ eV, $C_1 = -10.552$ eV Å^2, $C_2 = -12.134$ eV Å^2, $M_0 = -0.6362$ eV, $M_1 = -6.8653$, $M_2 = 4.7005$ eV Å^2, and $A = 2.7602$ eV Å. Evaluating the eigenvalues

$E(\mathbf{k}) = \epsilon_0(\mathbf{k}) \pm \sqrt{M(\mathbf{k})^2 + A^2 k_+ k_- + |B(\mathbf{k})|^2}$, we get a pair of gapless solutions at

$\mathbf{k}^c = (0, 0, k_z^c = \pm\sqrt{\frac{M_0}{M_1}})$, which are nothing but just the two Dirac points on the k_z axis discussed above.

As we only concentrate on the vicinity of each crossing point $\mathbf{k}^c$, we choose $\mathbf{k}^c$ for reference and define $\mathbf{q} = \mathbf{k} - \mathbf{k}^c = (q_x, q_y, q_z)$. By expanding the Hamiltonian near the reference

point and keeping only the linear order terms, we get

$$H^c(\mathbf{q}) = \begin{pmatrix} h(\mathbf{q}) & 0 \\ 0 & h^*(\mathbf{q}) \end{pmatrix}, \quad (1)$$

with

$$h(\mathbf{q}) = q_z(2C_1 k_z^c)\sigma_0 + q_x A\sigma_x - q_y A\sigma_y - q_z(2M_1 k_z^c)\sigma_z, \quad (2)$$

where σ_0 is the unit matrix and $(\sigma_x, \sigma_y, \sigma_z)$ are Pauli matrices. The linearized Hamiltonian around the $\mathbf{k}^c$ point is nothing but the 3D anisotropic massless Dirac fermions, which can be decoupled into two Weyl fermions with degenerate energy. The energy spectrum is $\varepsilon_\pm(\mathbf{q}) = T(\mathbf{q}) \pm U(\mathbf{q}) = 2C_1 k_z^c q_z \pm \sqrt{(Aq_x)^2 + (Aq_y)^2 + (2M_1 k_z^c q_z)^2}$. Inserting the parameters obtained above into the formula, we can clearly see that $T(\hat{q}_z) > U(\hat{q}_z)$ along the $\hat{q}_z$ axis. Hence, the Dirac cone tilts strongly along the $\hat{k}_z$ direction, which causes the Dirac point to appear at the point where the open electron and hole pockets touch [11]. The Dirac points in PtSe$_2$ are therefore type-II Dirac points. As Weyl semimetals can, in principle, be realized by breaking either time-reversal or inversion symmetries of Dirac semimetals, type-II Weyl fermions are expected to be accessible in PtSe$_2$-class materials by splitting type-II Dirac points using magnetic doping or external strains.

One of the most interesting phenomena of a Dirac semimetal is the presence of symmetry-protected surface states. We have computed the surface states for the (001) surface of PtSe$_2$, which are shown in Fig. 3. On the (001) surface, two Dirac points project to the $\bar{\Gamma}$ point of the surface BZ. According to previous analysis of conventional Dirac semimetals, such as Na$_3$Bi and Cd$_3$As$_2$ [1,2], there is just a single point on the Fermi surface of the (001) surface, and the signals of the surface bands depend sensitively on the surface potential [17]. However, for the type-II Dirac points in PtSe$_2$, we do find some surface bands (marked with green arrows) between bulk bands at the (001) surface as shown in Fig. 3(a). By investigating the evolution of the surface states of PtSe$_2$ under uniaxial strain, we find that the two surface states start from continuous bulk states, disperse upward,
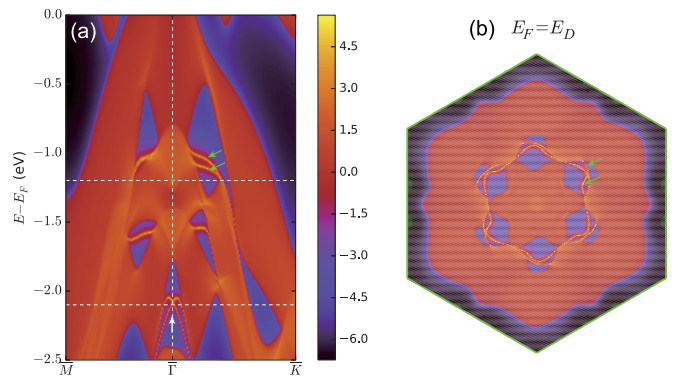

FIG. 3. The projected surface states and isoenergy surface for the (001) surface of PtSe$_2$. (a) The projected surface density of states for the (001) surface. The projected Dirac points are denoted by green dots. The green arrows mark surface states around the projected Dirac point, whereas the white arrows represent the Dirac-cone surface state due to nontrivial $\mathbb{Z}_2$ topology. (b) The isoenergy surface at E_D of the (001) surface.

and merge together at the projected Dirac point (for details of the calculation, see the Supplemental Material [31]). The isoenergy surfaces at $E_F = E_D$ make it clear that the two surface bands are located in the gapped circular region of the bulk-state continuum [Fig. 3(b)]. These surface states, which are related to the symmetry-protected Dirac points, would be affected significantly when the trigonal symmetry is broken (see the Supplemental Material [31]). In addition, due to the nontrivial $\mathbb{Z}_2$ topological gap between the v_3 and the v_4 valence bands, a Dirac-cone surface state lies deeply below the Fermi level around -2.1 eV and is well separated from bulk states in the (001) surface [see the white arrows in Fig. 3(a)]. These surface states should be experimentally measurable by a modern angle-resolved photoemission spectroscopy (ARPES) technique. In fact, similar novel surface states and type-II Dirac points of transition metal dichalcogendie PtTe₂ are observed in our recent ARPES measurements [35].

In conclusion, based on first-principles calculations and effective Hamiltonian analysis, we predict the existence of the type-II Dirac fermions that emerge at the boundary between electron and hole pockets in the transition metal dichalcogenide PtSe₂ class. A single pair of type-II Dirac points, which are protected by the trigonal rotation symmetry, exists on the k_z axis of the bulk BZ. Moreover, novel surface states and doping-driven Lifshitz transition are observable in these materials. Our Rapid Communication provides useful guidance for experimentally detecting type-II Dirac fermions and related intriguing physical properties in a family of transition metal dichalcogenides.

Note added in proof. In the final stages of preparing this Rapid Communication, we became aware of the independent work by Le *et al.* [36] and Chang *et al.* [37] which reported similar type-II Dirac fermions in KMgBi and VAl₃ family materials, respectively.

[1] Z. Wang, Y. Sun, X.-Q. Chen, C. Franchini, G. Xu, H. Weng, X. Dai, and Z. Fang, Phys. Rev. B **85**, 195320 (2012).

[2] Z. Wang, H. Weng, Q. Wu, X. Dai, and Z. Fang, Phys. Rev. B **88**, 125427 (2013).

[3] X. Wan, A. M. Turner, A. Vishwanath, and S. Y. Savrasov, Phys. Rev. B **83**, 205101 (2011).

[4] A. A. Burkov and L. Balents, Phys. Rev. Lett. **107**, 127205 (2011).

[5] H. Weng, C. Fang, Z. Fang, B. A. Bernevig, and X. Dai, Phys. Rev. X **5**, 011029 (2015).

[6] S.-M. Huang, S.-Y. Xu, I. Belopolski, C.-C. Lee, G. Chang, B.K. Wang, N. Alidoust, G. Bian, M. Neupane, C. Zhang *et al.*, Nat. Commun. **6**, 7373 (2015).

[7] J. Liu and D. Vanderbilt, Phys. Rev. B **90**, 155316 (2014).

[8] W. Cao, P. Tang, S.-C. Zhang, W. Duan, and A. Rubio, Phys. Rev. B **93**, 241117 (2016).

[9] H. B. Nielsen and M. Ninomiya, Phys. Lett. B **130**, 389 (1983).

[10] A. A. Abrikosov, Phys. Rev. B **58**, 2788 (1998).

[11] A. A. Soluyanov, D. Gresch, Z. Wang, Q. Wu, M. Troyer, X. Dai, and B. A. Bernevig, Nature (London) **527**, 495 (2015).

[12] Y. Sun, S.-C. Wu, M. N. Ali, C. Felser, and B. Yan, Phys. Rev. B **92**, 161107 (2015); S. Kourtis, J. Li, Z. Wang, A. Yazdani, and B. A. Bernevig, *ibid.* **93**, 041109 (2016); T.-R. Chang, S.-Y. Xu, G. Chang *et al.*, Nat. Commun. **7**, 10639 (2016); Z. Wang, D. Gresch, A. A. Soluyanov *et al.*, Phys. Rev. Lett. **117**, 056805 (2016).

[13] K. Deng, G. Wan, P. Deng *et al.*, Nat. Phys. (2016), doi:10.1038/nphys3871; L. Huang, T. M. McCormick, M. Ochi *et al.*, Nat. Mater. (2016), doi:10.1038/nmat4685; N. Xu, Z. J. Wang, A. P. Weber *et al.*, arXiv:1604.02116; A. Liang, J. Huang, S. Nie *et al.*, arXiv:1604.01706; J. Jiang, Z. K. Liu, Y. Sun *et al.*, arXiv:1604.00139.

[14] F. Y. Bruno, A. Tamai, Q. S. Wu *et al.*, Phys. Rev. B **94**, 121112(R) (2016); Y. Wu, D. Mou, N. H. Jo *et al.*, *ibid.* **94**, 121113(R) (2016); C. Wang, Y. Zhang, J. Huang *et al.*, arXiv:1604.04218.

[15] G. E. Volovik, arXiv:1604.00849.

[16] Y. Xu, F. Zhang, and C. Zhang, Phys. Rev. Lett. **115**, 265304 (2015).

[17] Z. K. Liu, B. Zhou, Y. Zhang *et al.*, Science **343**, 864 (2014); S.-Y. Xu, C. Liu, S. K. Kushwaha *et al.*, *ibid.* **347**, 294 (2015); J. Xiong, S. K. Kushwaha, T. Liang *et al.*, *ibid.* **350**, 413 (2015).

[18] M. Neupane, S.-Y. Xu, R. Sankar *et al.*, Nat. Commun. **5**, 3786 (2014); Z. K. Liu, J. Jiang, B. Zhou *et al.*, Nat. Mater. **13**, 677 (2014); S. Borisenko, Q. Gibson, D. Evtushinsky *et al.*, Phys. Rev. Lett. **113**, 027603 (2014).

[19] J. P. Perdew, K. Burke, and M. Ernzerhof, Phys. Rev. Lett. **77**, 3865 (1996).

[20] G. Kresse and J. Furthmüller, Comput. Mater. Sci. **6**, 15 (1996).

[21] N. Marzari and D. Vanderbilt, Phys. Rev. B **56**, 12847 (1997); I. Souza, N. Marzari, and D. Vanderbilt, *ibid.* **65**, 035109 (2001).

[22] A. A. Mostofi, J. R. Yates, Y.-S. Lee, I. Souza, D. Vanderbilt, and N. Marzari, Comput. Phys. Commun. **178**, 685 (2008).

[23] H. Huang, Z. Wang, N. Luo, Z. Liu, R. Lü, J. Wu, and W. Duan, Phys. Rev. B **92**, 075138 (2015).

[24] H. Huang, J. Liu, D. Vanderbilt, and W. Duan, Phys. Rev. B **93**, 201114 (2016).

[25] M. P. López Sancho, J. M. López Sancho, and J. Rubio, J. Phys. F **14**, 1205 (1984); **15**, 851 (1985).

[26] H. Huang, J. Liu, and W. Duan, Phys. Rev. B **90**, 195105 (2014).

[27] H. Huang, Z. Liu, H. Zhang, W. Duan, and D. Vanderbilt, Phys. Rev. B **92**, 161115 (2015).

[28] B. Bradlyn, J. Cano, Z. Wang, R. Cava, and B. A. Bernevig, Science **353**, 6299 (2016).

[29] H. Weng, C. Fang, Z. Fang, and X. Dai, Phys. Rev. B **93**, 241202 (2016); Z. Zhu, G. W. Winkler, Q. S. Wu, J. Li, and A. A. Soluyanov, Phys. Rev. X **6**, 031003 (2016).

[30] G. F. Koster, *Properties of the Thirty-Two Point Groups* (MIT Press, Cambridge, MA, 1963), Vol. 24.

[31] See Supplemental Material at http://link.aps.org/supplemental/10.1103/PhysRevB.94.121117 for Type-II Dirac fermions in the PtSe₂ class of transition metal dichalcogenides.

[32] A. A. Soluyanov and D. Vanderbilt, Phys. Rev. B **83**, 235401 (2011).

[33] Y. Liu, J.-Z. Zhao, Y. Li, C.-T. Lin, A.-J. Liang, C. Hu, Y. Ding, Y. Xu, S.-L. He, L. Zhao *et al.*, Chin. Phys. Lett. **32**, 067303 (2015).

[34] G. L. Bir and G. E. Pikus, *Symmetry and Strain-Induced Effects in Semiconductors* (Wiley, New York, 1974), Vol. 624.

[35] M. Yan, H. Huang, K. Zhang, E. Wang, W. Yao, K. Deng, G. Wan, H. Zhang, M. Arita, H. Yang, Z. Sun, H. Yao, Y. Wu, S. Fan, W. Duan, and S. Zhou, arXiv:1607.03643.

[36] C. Le, S. Qin, X. Wu, X. Dai, P. Fu, and J. Hu, arXiv:1606.05042.

[37] T.-R. Chang, S.-Y. Xu, D. S. Sanchez, S.-M. Huang, G. Chang, C.-H. Hsu, G. Bian, I. Belopolski, Z.-M. Yu, X. Xu *et al.*, arXiv:1606.07555.